



Original Research Article

Investigation of Optoelectronics, Thermoelectric, Structural and Photovoltaic Properties of $\text{CH}_3\text{NH}_3\text{SnBr}_3$ Lead-Free Organic Perovskites

Tomal Hossain¹, Md. Sayed Hossain², Md. Hazrat Ali¹, Unesco Chakma¹ , Ajoy Kumer^{3,4*} , Mohammad Jahidul Islam⁵

¹Department of Electrical and Electronics Engineering, European University of Bangladesh, Gabtoli, Dhaka-1216, Bangladesh

²Center for Research Reactor, Bangladesh Atomic Energy Commission, Dhaka, Bangladesh

³Department of Chemistry, European University of Bangladesh, Gabtoli, Dhaka-1216, Bangladesh

⁴Department of Chemistry, Bangladesh University of Engineering and Technology, Dhaka-1000, Bangladesh

⁵Department of Physics, European University of Bangladesh, Gabtoli, Dhaka-1216, Bangladesh

ARTICLE INFO

Article history

Submitted: 2021-03-28

Revised: 2021-04-21

Accepted: 2021-05-01

Manuscript ID: CHEMM-2103-1324

Checked for Plagiarism: Yes

Language Editor:

Dr. Behrouz Jamalvandi

Editor who approved publication:

Dr. Vahid Khakyzadeh

DOI: 10.22034/chemm.2021.130180

KEYWORDS

Band gap

DOS

PDOS

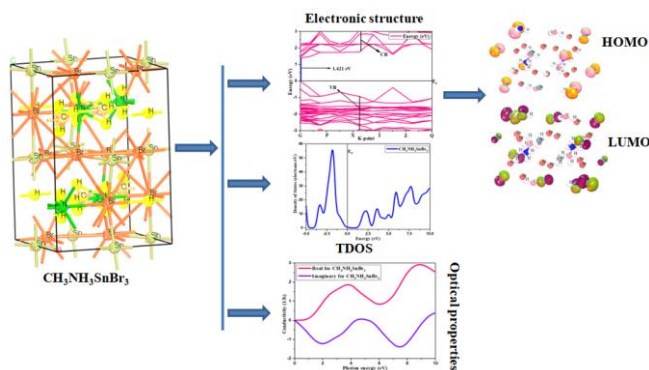
Optoelectronics and organic

perovskites

ABSTRACT

To develop the lead-free organic perovskites, the crystal $\text{CH}_3\text{NH}_3\text{SnBr}_3$ was selected for their computational exploration which has a vast functional application in optoelectronic area as functional materials. First of all, the electronics band structures, the total density of state, the partial density of state and optical properties were investigated by DFT functional for $\text{CH}_3\text{NH}_3\text{SnBr}_3$. In general, the band gap of $\text{CH}_3\text{NH}_3\text{SnBr}_3$ was calculated at 1.421 eV by Generalized Gradient Approximation (GGA) with Perdew Burke Ernzerhof (PBE) functional, and the energy gap and open circuit voltage was evaluated. The density of states (DOS) and partial density of states (PDOS) were evaluated to show that how each atom can be contributed to their electronic structure. The optical properties, for instance absorption, reflection, refractive index, conductivity, dielectric function, and loss function were estimated. Further, Sn atom was substituted to design the lead-free molecule, $\text{CH}_3\text{NH}_3\text{SnBr}_3$ that passed good optoelectronic and optical properties. It can be concluded that Sn atoms containing organic crystal, $\text{CH}_3\text{NH}_3\text{SnBr}_3$, show narrow band gap in comparison to lead or other heavy metals containing crystals although Sn is smaller in atomic size than Pd atom.

GRAPHICAL ABSTRACT



* Corresponding author: Ajoy Kumer

✉ E-mail: kumarajoy.cu@gmail.com

© 2020 by SPC (Sami Publishing Company)

Introduction

Perovskites are generally in the shape of orthorhombic, of which the structural formula is ABX_3 (A =organic ammonium cation acted as ligand with metal in complex, $CH_3NH_3^+$; B = Sn^{2+} or other metals; X = Cl^- , Br^- , I^-) [1-3]. The electrical and optical features of Pb-based perovskites has expressed approximately perfect solar cells [4, 5]. Perovskites solar cell's latest efficiency has reached 23.7% [6, 7], which exceeds $Cu(In,Ga)(Se,S)_2$, CdTe and Si-based solar cells [8, 9]. Nevertheless, two main concerns of Pb-based perovskites solar cells are: Poor stability and high toxicity [10, 11]. The stability challenge of these perovskites is undertaken by using two-dimensional (2D) perovskites, as well as advanced device encapsulation and engineering applications [12, 13]. The development of less toxic Pb-free materials is certainly always a priority in the solar cell market even if performance is not compromised much. Ideal Pb-free candidates as solar cell absorbers should have less toxicity, narrow direct band gaps [14], high optical-absorption coefficients [15], high mobility [16], low exciting-binding energies [17], longer charge-carrier life times, and good stability [18, 19]. Further they have interesting features including less-toxicity constituents for making perovskite structures, such as Sn/Ge-based halides [20], some double perovskites [21, 22], and some Bi/Sb-based halides [23] with perovskite-like structure.

Among these contestants, Sn-based perovskites have attracted the most attention because of their custom-made properties and the most promising performance achieved by their devices [24]. The direct band gaps of around 1.20 eV, 1.41 eV and 1.3 eV for the representative methylammonium tin iodide ($MA\text{SnI}_3$) [25], formamidinium tin iodide ($FASnI_3$) [26], and cesium tin iodide ($CsSnI_3$) [27], respectively, which are even narrower and more attractive than those of their Pb-based analogs. After being exposed to the air in the atmosphere, Sn-based Perovskites Sn^{4+} became SnO_2 that is an eco-friendly material [28]. A quick inspection of all

the basic physical features of Sn-based perovskites reveals a significant similarity by making a comparison with Pb-based ones [29]. Therefore, at least in principle these materials should be able to match the photovoltaic properties of the ABX_3 (such as $APbI_3$) elements. After the first report on Sn-based perovskite solar cells which achieved about 6% power conversion efficiency (PCE) [30], many reports have focused on Sn-based perovskites solar cells. It has been reported that 9.6% is the highest efficiency of Sn-based perovskites solar cells. Keeping an eye on photovoltaic parameters, Sn-based perovskites solar cells usually have high short-circuit current densities of 20 to 25 mA cm^{-2} due to their low band gaps [31]. However, the average of open-circuit voltage (V_{oc}) of the Pb-based analogs is 1.1 V whereas the average of open-circuit voltage (V_{oc}) of the solar cells is only around 0.5 V, which is much lower in value [32]. Heavy P-type doping of materials is the major reason for the lower V_{oc} of Sn-based perovskites solar; heavy doping is responsible for the highly complex and unwanted oxidization of Sn^{2+} to Sn^{4+} [33, 34], which works as a P-type dopant in the structure resulting in excessively high dark-carrier concentration and very high photo carrier recombination.

It has been recently found that, adding ethylenediammonium (EN) cations gives birth to a new type of three-dimensional (3D) so-called hollow perovskites of Sn-based perovskites [6], which can tune the band gap from 1.3 to 1.9 eV [35]. As a result, with the of addition 10% EN the 3D hollow Sn-based perovskites solar cells achieved a much higher V_{oc} 's and PCEs than the standard $ASnI_3$ perovskites (0.48 V and 7.14% vs. 0.15 V and 1.4%) [6].

A recent study achieved 9.6% recorded efficiency by adding 1% en combining 20% guanidinium (GA) [36]. Other cations, such as phenylethylammonium (PEA) and butylammonium (BA), are also attractive in low-dimensional structures. The representatives of 2D $(PEA)_2(MA)_{n-1}Sn_nI_{3n+1}$ and $(BA)_2(MA)_{n-1}Sn_nI_{3n+1}$ perovskites have much better stability

due to protecting the organic gap levels. In particular, recent reports have described that high performance typically uses 2D Sn-based perovskites with a reverse device structure, with the highest PCE providing 9.4%. In the Sn-based perovskites solar cells, using both 3D hollow and 2D perovskites in the same films may significantly progress the stability. The most stable of Sn-based perovskites is Cs_2SnX_6 (X =I, Br) which is a peculiar compound having a stable Sn^{4+} . Therefore, it does not oxidize. The major disadvantage is that it does not have a fully 3D perovskites structure. Cs_2SnI_6 has a narrow direct band gap of 1.3 to 1.6 eV [37].

These materials have been used in different kinds of optoelectronic devices, including solar cells [20, 38], light-emitting diodes (LED) [39], lasers [40, 41], photo detectors [42], photocatalysis [43-46], electric device [44, 47-51] and even chemo sensors [52]. Comparing with commercial silicon-based photo detectors, the perovskites photo detectors have demonstrated superior performance and application prospects. Recent research shows an ultra-high response exceeding 10^4 AW^{-1} and a short response time of $<1\text{ns}$ was achieved in a short of time. A visible photodetector based on perovskites can reach a photoconductive gain of 10^4 electrons per photon [42, 53].

No theoretical studies are available for characterization of $\text{CH}_3\text{NH}_3\text{SnBr}_3$, according to the best of our knowledge. This paper covers the complementary study of $\text{CH}_3\text{NH}_3\text{SnBr}_3$ including the detailed investigation of structural, electronic and optical and thermodynamic properties using first principles-based Density Functional Theory (DFT). We also report, for the first time, the main features including band gap energy, ionized donor density, etc. which are studied on the basis of the absorption spectra and polarization curves.

In this study, band structure has been studied using GGA with PBE method which has been considered the most accurate functional from computational tools. Secondly, it illustrates that how the s, p and d orbitals contribute in valance

band and conduction band even band gap. Finally, it can be said that $\text{CH}_3\text{NH}_3\text{SnBr}_3$ is an eco-friendly material and its optical properties are accounted as best supportive properties for light absorption and can be used as photovoltaic cell.

Material and methods

Initially, the geometric optimization was achieved before energy calculation where the convergence criterion for the force between atoms was $3 \times 10^{-6} \text{ eV/\text{Å}}$, and the maximum displacement, the total energy and the maximal stress were at $1 \times 10^{-3} \text{ \AA}$, $1 \times 10^{-5} \text{ eV/atom}$ and $5 \times 10^{-2} \text{ GPa}$, respectively. After geometry stabilization through molecular optimization, the method of GGA with PBE functional was used from CASTEP code of the material studio version 8.0 [54] for calculating the electronic band structure, total density of state (TDOS) and partial density of state (PDOS), because this functional has been considered the most feasible method for calculating the electronic and structural properties [55]. In this condition, the band structure and density of state were enumerated using the cut off at 500 eV, and k point at $2 \times 2 \times 2$ with norm-conserving pseudopotentials. Next, the optical features, such as refractive index, reflectivity, absorption, conductivity and loss function, were similarly simulated for calculation. In addition, for the comparative study of band gaps for $\text{CH}_3\text{NH}_3\text{SnBr}_3$, the Generalized Gradient Approximation (GGA) with Perdew-Burke-Ernzerhof (PBE) [56] functional was investigated using required cut off energy at 500 eV, and k point at $2 \times 2 \times 2$ with nom-conserving pseudopotentials of required structures.

Result and Dissection

Geometry of optimized structure

The lattice parameters value for $\text{CH}_3\text{NH}_3\text{SnBr}_3$ are $a = 8.422 \text{ \AA}$, $b = 8.547 \text{ \AA}$, $c = 12.184 \text{ \AA}$ and angles between them as $\alpha = 90.000^\circ$, $\beta = 90.000^\circ$, $\gamma = 90.000^\circ$. The $\text{CH}_3\text{NH}_3\text{SnBr}_3$ crystal and the space group is Hermann Mauguin Pnma [62], orthorhombic crystal system, point group mmm,

hall -P 2ac 2n, density 3.63 g/cm³ shown in figure 1. The optimized structure of materials showing in from the materials studio after optimizing their crystal structure.

Opto-electronic properties

Electronic structure

The electronic band gap plays significant role of semiconductor for determining the color and conductivity of materials to reveal their absorption capacity of visible or UV and ultraviolet light. The maximum valence band (MVB) and the minimum conduction band (MCB) is closely attribute to the Lowest Unoccupied Molecular Orbital (LUMO) and Highest Occupied Molecular Orbital (HUMO) are shown in figure 2 and figure 3. The energy range of the band gap 1.1 eV to 1.5 eV that absorb all color of visible light. The Fermi energy level has been set at 0 eV for determining the electronic band structure of CH₃NH₃SnBr₃ as shown in figure 4. The band gap has been reported 1.421 eV using the most accurate GGA with PBE method. It has been observed that higher energy state of valence band was in found in G symmetry point as well as the lower energy state of conduction was obtained in G point that reveals it follows the nature of direct band gap so that the electron can easily shift maximum valence band to the minimum conduction band without changing the momentum.

Density of states and Partial density of state

The method GGA with PBE has been applied to evaluate the density of states (DOS) or partial density of states (PDOS) of CH₃NH₃SnBr₃ compound for determining the nature of electronic structure properly as well as scattering of orbital. Figures 5 to 10 depict the total density of states and partial density of states as a function of photon energy that are closely related the Highest Occupied Molecular Orbital (HOMO), Lowest Unoccupied Molecular Orbital (LUMO) and $E_{\text{HOMO}} - E_{\text{LUMO}}$ gap. In Figure 6, for PDOS of CH₃NH₃SnBr₃ it consists of 2p² for C, 1s¹ for H, 2p³ for N, 5p² for Sn, and 4p⁵ for Br

atoms. It has been found that the highest electron density in the valence band at about 55 electrons/ eV for p orbital and s orbital provide some contribution bellow Fermi energy. In the conduction band, the strong contribution of hybridization provides 5p² for Sn atom in the photon energy range between 1 eV to 5 eV, also 2p³ orbital for N atom is provide moderate contribution. So that Sn metal is responsible for lower energy band gap which is a crucial point in this research. Finally, it can be seen that the p orbital is the higher contributor for both valence and conduction band of CH₃NH₃SnBr₃ lead free perovskites. Figures 7 to 10 represent the comparative study of s, p, and d orbitals for CH₃NH₃SnBr₃.

To compare its opto-electronic properties for CH₃NH₃SnBr₃ in case of electronic structure is very close to CsSnCl₃, CsPbBr₃, CH₃NH₃PbBr₃, NH₂CHNH₂SnBr₃ which was estimated as opto-electronic materials [57].

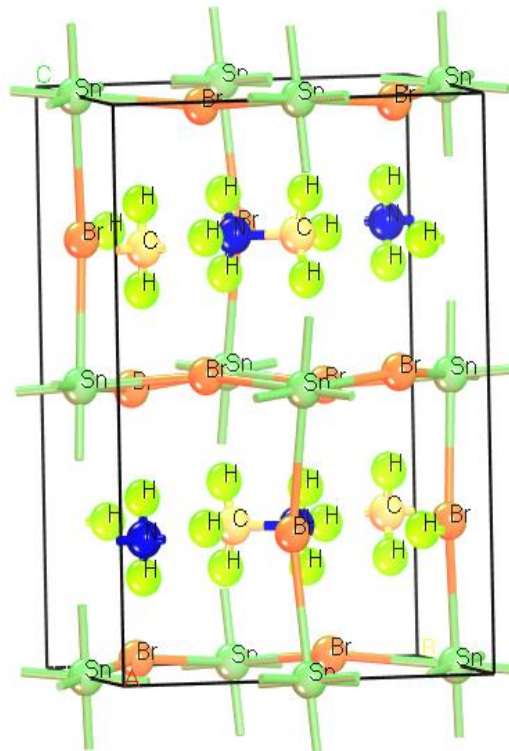


Figure 1: Optimized structure of CH₃NH₃SnBr₃

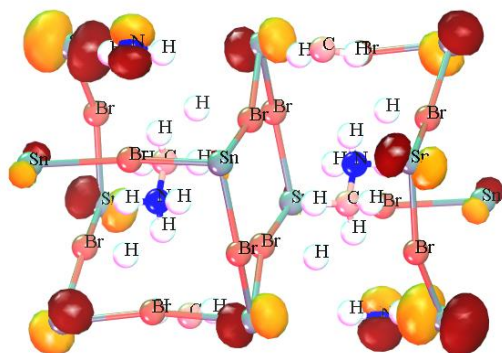


Figure 2: LUMO (CB)

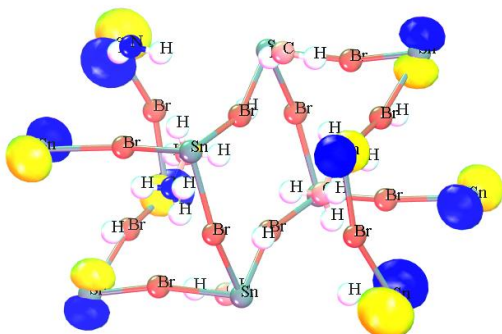


Figure 3: HOMO (VB)

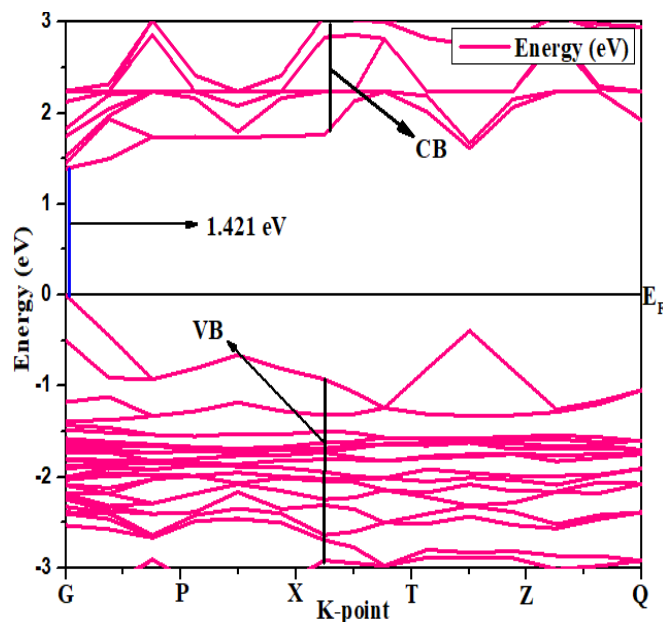


Figure 4: Electronic structure for $\text{CH}_3\text{NH}_3\text{SnBr}_3$

Note:

- For HOMO, Blue color indicates the positive node and yellow color mentions the negative color of orbital.
- In case of LUMO, deep radish color is positive and deep orange is negative.
- CB = Conduction band and VB = Valance band.

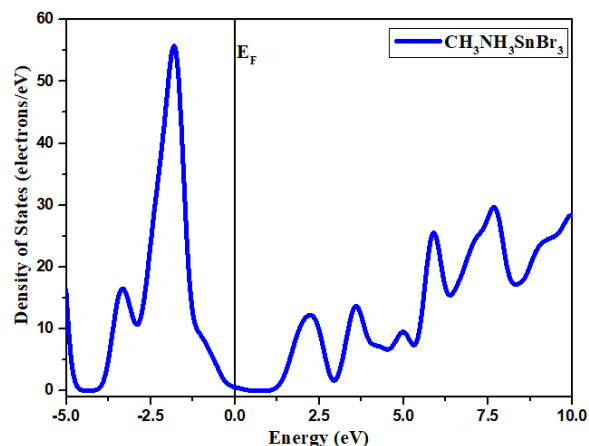


Figure 5: Total density of states

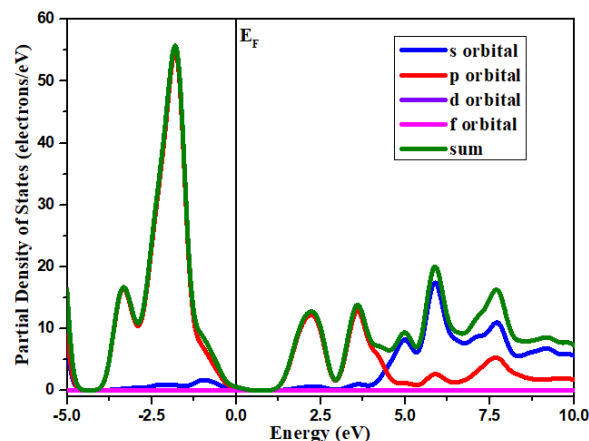


Figure 6: Partial density of states

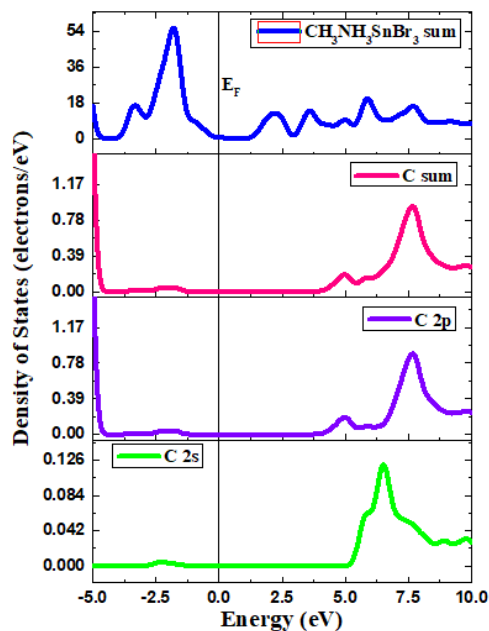
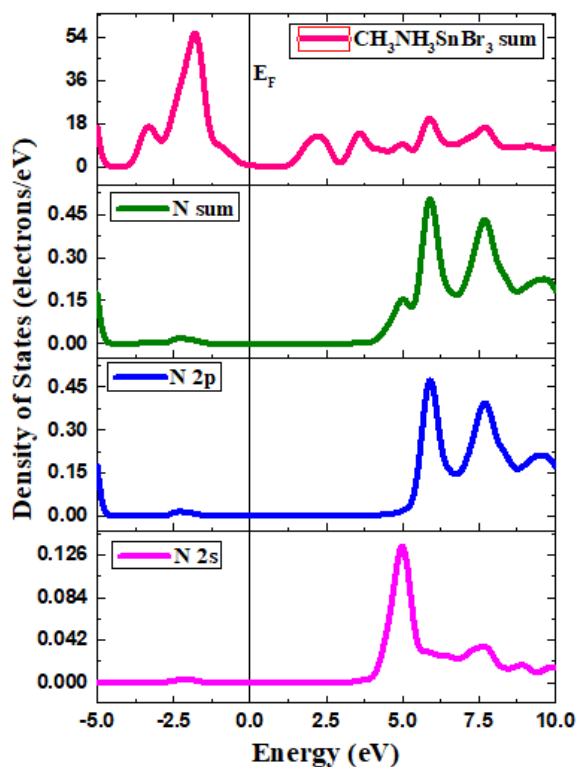
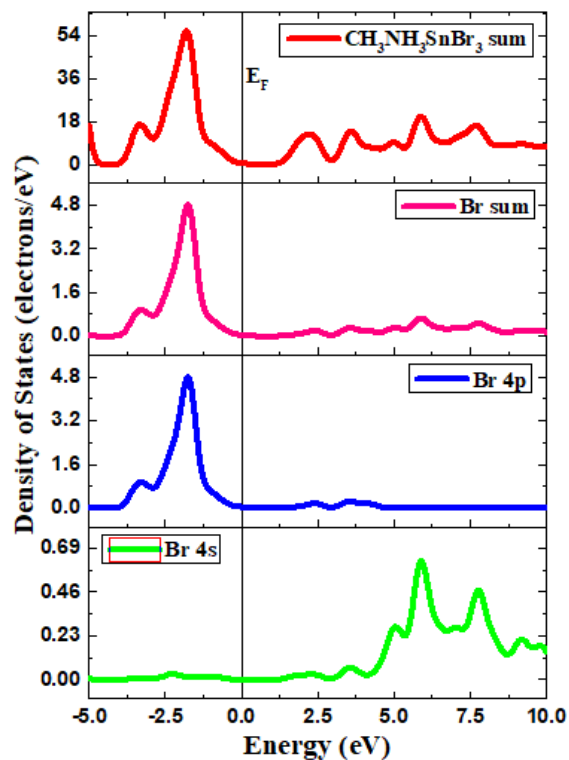
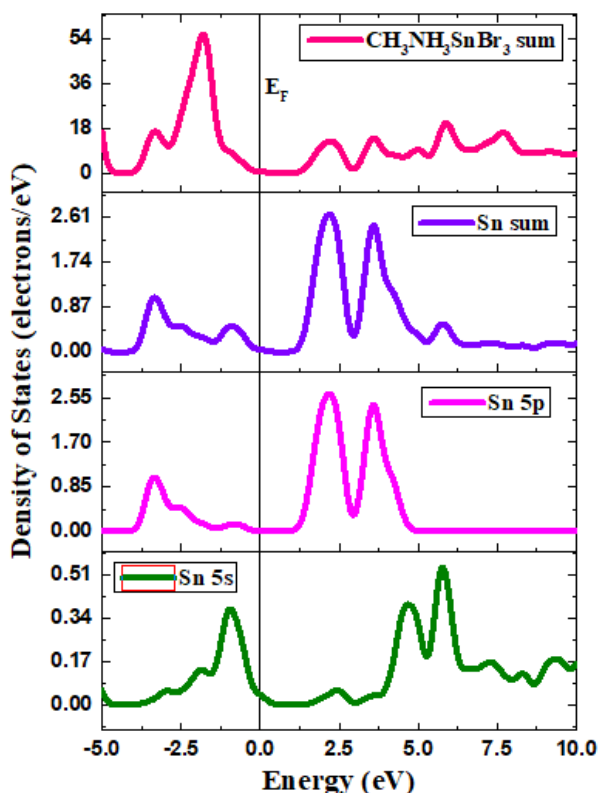


Figure 7: C atom for $\text{CH}_3\text{NH}_3\text{SnBr}_3$

Figure 8: N atom for CH₃NH₃SnBr₃Figure 10: Br atom for CH₃NH₃SnBr₃Figure 9: Sn atom for CH₃NH₃SnBr₃

Photovoltaic and chemical properties

As one of the most important properties of photovoltaic, maximum open circuit voltage (V_{oc}) may be defined as electrical potential difference between two ends of an electric device or materials. When it has been disconnected from any circuit, it has to be related the term of HOMO and LUMO of the organic solar cell. In addition, it is the difference of HOMO and LUMO or energy gap between valance band and conduction band into account the energy lost during the photo-charge generation. The mathematical expression for calculating the magnitudes of open-circuit voltage (V_{oc}) has been calculated from the following equation:

In addition, according to Koopman's theorem for energy gap, E_{gap} is defined as the difference between HOMO and LUMO energy [58]. The ionization potential (I), and electron affinity (A) can be estimated from the HOMO and LUMO energy values. The HOMO and LUMO energies are used for the determination of global reactivity descriptors. The electrophilicity (ω),

chemical potential (μ), electronegativity (χ), hardness (η) and softness (S) are calculated

| Table 1: Data of HOMO, LUMO, chemical descriptors, Open circuit voltage | | Formula |
|-------------------------------------------------------------------------|--------|--------------------------------------------------------------------------------------|
| HOMO, eV | -5.256 | |
| LUMO, eV | -3.830 | |
| ΔE , (LUMO-HOMO) gap | 1.426 | $E_{\text{gap}} = (E_{\text{LUMO}} - E_{\text{HOMO}}) \approx \text{IP} - \text{EA}$ |
| Ionization potential (I), eV | 5.256 | $I = -E_{\text{HOMO}}$ |
| Electron affinity (A), eV | 3.830 | $A = -E_{\text{LUMO}}$ |
| Hardness, (η) | 0.713 | $(\eta) = \frac{I - A}{2}$ |
| Softness, (S) | 1.402 | $(S) = \frac{1}{\eta}$ |
| Electrophilicity (ω), | 14.472 | $(\omega) = \frac{\mu^2}{2\eta}$ |
| Chemical potential, (μ) | -4.543 | $(\mu) = -\frac{I + A}{2}$ |
| Electronegativity, (χ) | 4.543 | $(\chi) = \frac{I + A}{2}$ |
| Open circuit voltage (V_{oc}), eV | -1.726 | $V_{\text{oc}} = E_{\text{HOMO}}(D) - E_{\text{LUMO}}(A) - 0.3$ |

To explain the chemical properties of this crystal, the LUMO-HOMO gap is to be mentioned for their chemical stability. For the organic compound, the LUMO-HOMO gap is 7.0 to 9.0 eV (59-64), indicating chemical stable configuration or molecule while this crystal illustrating the LUMO-HOMO gap is 1.426 eV as shown in Table 1. It is well known that the smaller LUMO-HOMO gap indicates the greater chemical stability of molecules. Moreover, the chemical potential, hardness and softness are also indicator of chemical stability while softness provides how easily dissociated or break down a molecule while hardness is completely opposite of softness. From Table 1, the large value of softness mentions its high chemical stability whereas the value of hardness inverses to softness.

Optical properties

Understanding about the interaction of incident electromagnetic radiation to a material belonging to towering applicable and informative tools is for proper use in optoelectronic devices. So, the optical analysis of various features, optical

reflectivity, optical absorption, optical reflective index, optical conductivity, optical dielectric function and loss function, enable us to appraise the compound repercussion with the electromagnetic wave and its electronic structure.

Optical reflectivity

To explain the nature of optoelectronic materials, the optical reflectivity plays a significant role about passing light through the materials when light falls on these materials that is explained in the following way. Firstly, UV light is exposed to these materials, it can absorb the light, and it can be considered that a smaller value of reflectivity illustrated greater absorption of light or UV. In this section, it was observed that the reflectivity of $\text{CH}_3\text{NH}_3\text{SnBr}_3$ crystal showed (Figure 11) that the value of reflectivity near photon energy 0 eV was around 0.18, representing no band gap was found in the Fermi energy level that confirmed $\text{CH}_3\text{NH}_3\text{SnBr}_3$ has a semi-conductor nature as organic perovskites cell. It is illustrated that the values of reflectivity for $\text{CH}_3\text{NH}_3\text{SnBr}_3$ maintain

the high reflectivity around the photon energy range about 1.40 eV at 0.22.

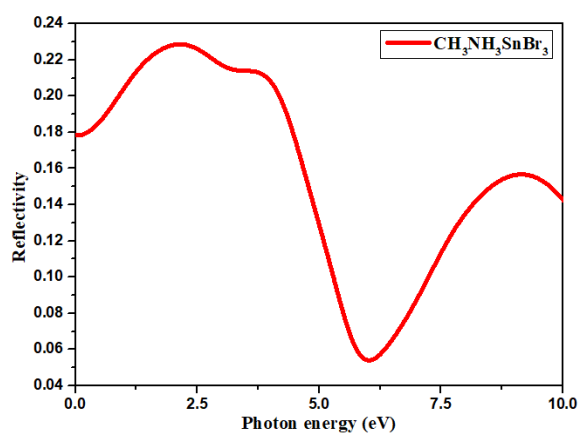


Figure 11: Optical Reflectivity

Optical absorption

Figure 12 illustrates that the study of the optical absorption for $\text{CH}_3\text{NH}_3\text{SnBr}_3$ is essential to provide information about polycrystalline polarization technique. It is revealed that absorption peaks are attributed to the transition energy from the highest energy states of valence band to the lowest energy state of conduction band under UV or visible light illumination. The maximum absorption was found for $\text{CH}_3\text{NH}_3\text{SnBr}_3$ crystal in the mid visible range between 3.10 eV and 8.20 eV.

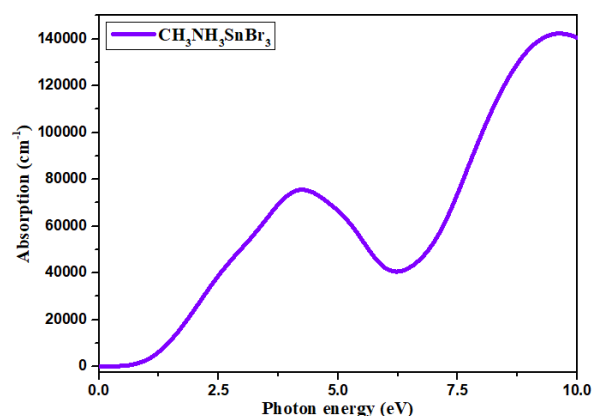


Figure 12: Optical Absorption

Optical reflective index

The refractive index has two segment real portion and imaginary portion. The real part of refractive index indicates the phase velocity whereas the imaginary segment is mass

attenuation coefficient. Figure 13 portrays the theoretical learning of refractive index as a function of photon energy reveals that the values for the imaginary part are almost zero until photon energy 6 eV for $\text{CH}_3\text{NH}_3\text{SnBr}_3$, although, at initial point of photon energy, the values of refractive index are at around 2.7 for real part for $\text{CH}_3\text{NH}_3\text{SnBr}_3$ organic crystal.

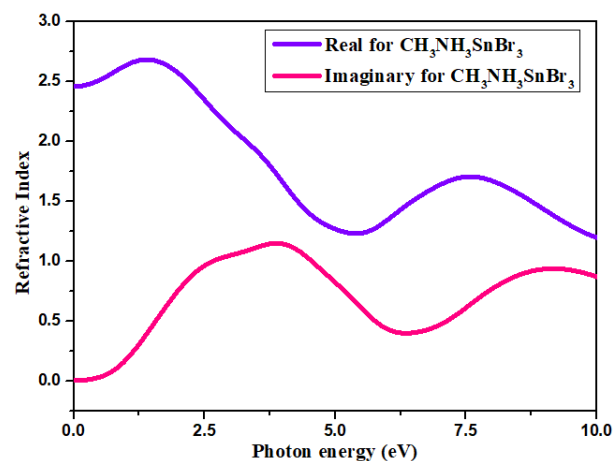


Figure 13: Optical Refractive Index

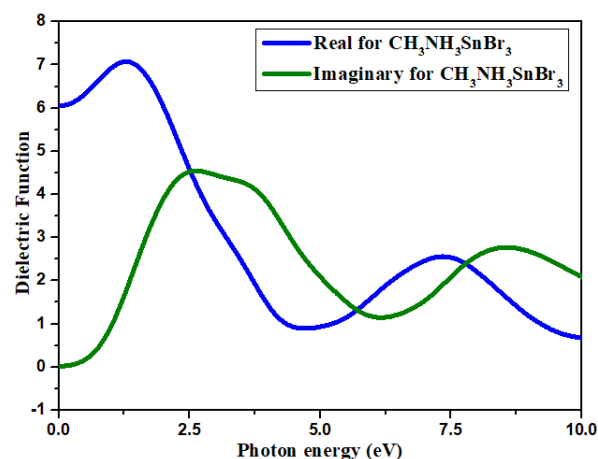


Figure 14: Optical Dielectric Function

Optical Dielectric Function

The dielectric function or relative permittivity is a significant tool to investigate their optical properties which is related with adsorption properties as following equation for solid [65, 66].

$$\varepsilon = \varepsilon_1(\omega) + i\varepsilon_2(\omega)$$

Here, ω is the light frequency, $\varepsilon_1(\omega)$ is a real part related to the electronic polarizability and

$\epsilon_2(\omega)$ is the imaginary part related to the electronic absorption of the material. The band structure of any material is the probability of photon absorption, which is closely related to the imaginary segment of dielectric function. The real part of the dielectric function shows the energy storing capacity and the energy attenuation capability for nonconductor materials. It can be seen from figure 14, the dielectric function starts from 7.1 for real part of $\text{CH}_3\text{NH}_3\text{SnBr}_3$ at 0 eV and changes steadily with changing photon energy at around 3 eV. However, the imaginary part shows zero dielectric function up to 3.5 eV for the organic crystal.

Optical Conductivity

The optical conductivity of the semiconductor on the basis of the energy band and free electrons is linked with the discrete space of electrons in orbit. This is also produced due to the presence of holes and free electrons in the crystal molecules. Figure 15 represents the optical conductivity changes with rising photon energy for $\text{CH}_3\text{NH}_3\text{SnBr}_3$. It can be seen that the value of the imaginary part of conductivity decreased exponentially with changing photon energy for $\text{CH}_3\text{NH}_3\text{SnBr}_3$ even that the initial value was zero at 0 eV. However, the higher optical conductivity value photon energy was 3.9 eV and 8.20 eV for $\text{CH}_3\text{NH}_3\text{SnBr}_3$ organic crystal.

Loss function

Loss function is an important characteristic of any substance by which it is understood how much energy the substance loses when dealing with optical properties, and two such substances come out. The first is called lower energy region and the second is called higher energy region. Figure 16 shows that the given object has zero value of its loss function at zero energy i.e. no energy is wasted from any system of the object. But as the energy increases, the loss function value of the object increases, which means that the application of high energy results in optical energy loss from the object, but as the photo

energy reaches 5, its value decreases again. This means that the optimized loss function is found in 5.0 eV because it has given the highest peak spectrum in this power.

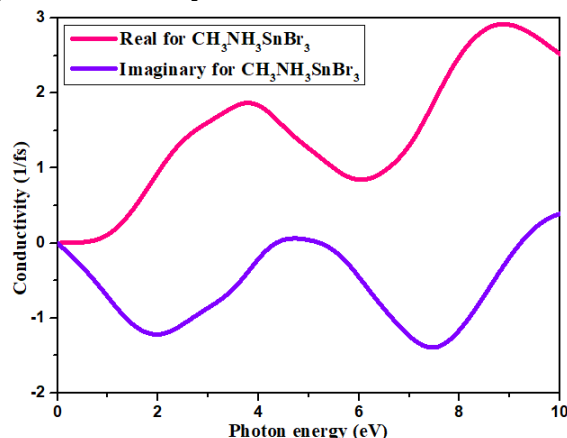


Figure 15: Optical Conductivity

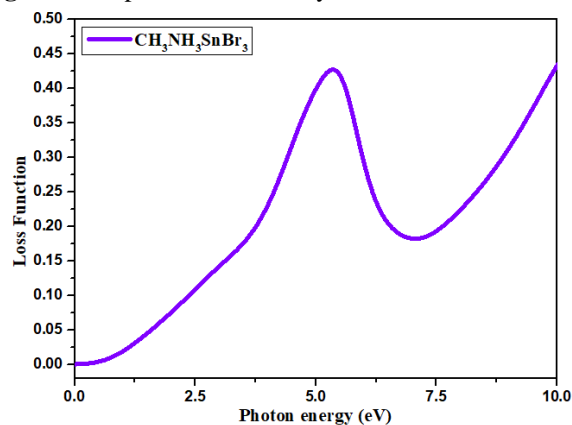


Figure 16: Optical Loss Function

Thermo-electric properties

The thermo-electric properties consist of entropy, heat capacity, enthalpy and free energy which are most significant for their uses in macroscopic physical systems, physical and chemical processes [67], biological system [68], conservation of energy [69] and electronic devices [70]. Entropy is a core conception [71] in physical chemistry, helping to measure the disorder of a system [72]. It was found that the entropy was increased with raising the temperature shown in figure 17. On the other hand, heat capacity plays a significant role of thermodynamics and is defined as material properties that changes with temperature and pressure. The comparison calculated data for heat capacity of metal-halide perovskites (MHPv)

is shown in Table 2. It indicates that the electrical conductivity changes for increasing temperature

shows a higher value owing to the heat capacity of MHPv at high temperature [73].

Table 2: Data of thermo-electric properties

| Temperature (K) | Entropy (cal/K/mol) | Heat Capacity (cal/K/mol) | Enthalpy (Kcal/mol) |
|-----------------|---------------------|---------------------------|---------------------|
| 100 | 106.7654 | 76.9906 | 3.204452 |
| 150 | 144.8432 | 110.3229 | 7.956346 |
| 200 | 179.6838 | 131.4549 | 14.03717 |
| 250 | 210.6544 | 145.8248 | 20.99026 |
| 300 | 238.2132 | 156.3508 | 28.5561 |
| 350 | 262.9745 | 164.9259 | 36.59323 |
| 400 | 285.5097 | 172.712 | 45.03585 |
| 450 | 306.291 | 180.313 | 53.86155 |
| 500 | 325.6836 | 187.9591 | 63.06802 |
| 550 | 343.959 | 195.6674 | 72.65855 |

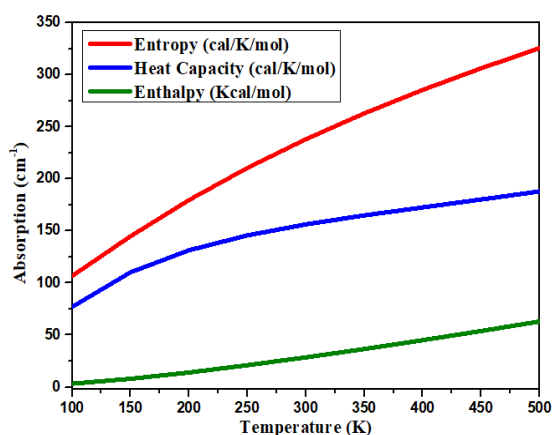


Figure 17: Thermo-electric properties

Conclusion

The calculated band gap of $\text{CH}_3\text{NH}_3\text{SnBr}_3$ is 1.421 eV through the method of GGA with PBE. On base structural geometry of orthorhombic, ABX_3 , $\text{CH}_3\text{NH}_3\text{SnBr}_3$ has been redesigned to make organic perovskites cell materials which are lead-free and smaller organic containing light materials, and shows low band gap. The optimized structure of $\text{CH}_3\text{NH}_3\text{SnBr}_3$ contains the space group Pnma which is the most stable configuration though it has shown the direct band gap organic perovskites. From the electrochemical analysis, the open circuit voltage has calculated at -1.726 eV while the standard value is 2.0 eV or below. According to band gap, it is similar to LUMO-HOMO gap, 1.426 eV, supporting the theoretical new development of lead-free organic perovskites, $\text{CH}_3\text{NH}_3\text{SnBr}_3$.

Moreover, it passes to obtain good optical absorbers, good optical conductivity and optical reflectivity influencing on direct band gap. The optoelectronic, electronic structure and optical properties give the strong evidences for use of new functional materials in photovoltaic, photocatalysis, photo detectors, light-emitting devices, piezoelectric, and magneto electrics

Funding

Authors declared that we did not receive any kind of funding from university or any institution.

Authors' contributions

All authors contributed toward data analysis, drafting and revising the paper and agreed to be responsible for all the aspects of this work.

Conflict of Interest

We have no conflicts of interest to disclose.

References

- [1]. Zhang Y., Ye H.Y., Zhang W., Xiong R.G., *Inorg. Chem. Front.*, 2014, **1**:118
- [2]. Reid A.F., Ringwood, A.E., *J. Geophys. Res.*, 1969, **74**:3238
- [3]. Liao W.Q., Ye H.Y., Zhang Y., Xiong R.G., *Dalton Trans.*, 2015, **44**:10614
- [4]. Kim B.G., Cho S.M., Kim T.Y., Jang H.M., *Phys. Rev. Lett.*, 2001, **86**:3404
- [5]. Chen P., Ong W.J., Shi Z., Zhao X., Li N., *Adv. Funct. Mater.*, 2020. **30**:1909667

- [6]. Ke W., Spanopoulos I., Tu Q., Hadar I., Li X., Shekhawat G.S., Dravid V.P., Kanatzidis M.G., *J. Am. Chem. Soc.*, 2019, **141**:8627
- [7]. Wang Z.K., Li M., Yang Y.G., Hu Y., Ma H., Gao X.Y., Liao L.S., *Adv. Mater.*, 2016, **28**:6695
- [8]. Koishiyev G.T., Sites J.R., Kulkarni S.S., Dhare N.G., *Determination of back contact barrier height in Cu (In, Ga)(Se, S)₂ and CdTe solar cells*. Presented at 2008 33rd IEEE Photovoltaic Specialists Conference, 2008
- [9]. Romeo A., Terheggen M., Abou-Ras D., Bätzner D.L., Haug F.J., Kälin M., Rudmann D., Tiwari A.N., *Prog. Photovoltaics*, 2004, **12**:93
- [10]. Su P., Liu Y., Zhang J., Chen C., Yang B., Zhang C., Zhao X., *J. Phys. Chem. Lett.* 2020, **11**:2812
- [11]. Fan Y., Xu Z., Huang Y., Wang T., Zheng S., DePasquale A., Brüeckner C., Lei Y., Li B., *J. Hazard. Mater.*, 2020, **400**:123299
- [12]. Zhang F., Lu H., Tong J., Berry J.J., Beard M.C., Zhu K., *Energy Environ. Sci.*, 2020, **13**:1154
- [13]. Ortiz-Cervantes C., Carmona-Monroy P., Solis-Ibarra D., *ChemSusChem*, 2019, **12**:1560
- [14]. Slavney A.H., Leppert L., Saldivar Valdes A., Bartesaghi D., Savenije T.J., Neaton J.B., Karunadasa H.I., *Angew. Chem., Int. Ed.*, 2018, **57**:12765
- [15]. De Wolf S., Holovsky J., Moon S.J., Löper P., Niesen B., Ledinsky M., Haug F.J., Yum J.H., Ballif C., *J. Phys. Chem. Lett.*, 2014, **5**:1035
- [16]. Kim H.J., Kim U., Kim H.M., Kim T.H., Mun H.S., Jeon B.G., Hong K.T., Lee W.J., Ju C., Kim K.H., Char K., *Appl. Phys. Express*, 2012, **5**:061102
- [17]. Chakraborty R., Nag A., *J. Phys. Chem. C*, 2020, **124**:16177
- [18]. Sun Q., Yin W.J., *J. Am. Chem. Soc.*, 2017, **139**:14905
- [19]. Wang R., Mujahid M., Duan Y., Wang Z.K., Xue J., Yang Y., *Adv. Funct. Mater.*, 2019, **29**:1808843
- [20]. Ito N., Kamarudin M.A., Hirotnani D., Zhang Y., Shen Q., Ogomi Y., Iikubo S., Minemoto T., Yoshino K., Hayase S., *J. Phys. Chem. Lett.*, 2018, **9**:1682
- [21]. Yin W.J., Weng B., Ge J., Sun Q., Li Z., Yan Y., *Energy Environ. Sci.*, 2019, **12**:442
- [22]. Howard C.J., Kennedy B.J., Woodward P.M., *Acta Crystallogr. Sect. B: Struct. Sci., Cryst. Eng. Mater.*, 2003, **59**:463
- [23]. Liu Z., Zhao X., Zunger A., Zhang L., *Adv. Electron. Mater.*, 2019, **5**:1900234
- [24]. Dong J., Shao S., Kahmann S., Rommens A.J., Hermida-Merino D., ten Brink G.H., Loi M.A., Portale G., *Adv. Funct. Mater.*, 2020, **30**:2001294
- [25]. Li F., Zhang C., Huang J.H., Fan H., Wang H., Wang P., Zhan C., Liu C.M., Li X., Yang L.M., Song Y., *Angew. Chem. Int. Ed.*, 2019, **58**:6688
- [26]. Schueller E.C., Laurita G., Fabini D.H., Stoumpos C.C., Kanatzidis M.G., Seshadri R., *Inorg. Chem.*, 2018, **57**:695
- [27]. Han J.S., Le Q.V., Choi J., Kim H., Kim S.G., Hong K., Moon C.W., Kim T.L., Kim S.Y., Jang H.W., *ACS Appl. Mater. Interfaces*, 2019, **11**:8155
- [28]. Hong J.A., Jung E.D., Yu J.C., Kim D.W., Nam Y.S., Oh I., Lee E., Yoo J.W., Cho S., Song M.H., *ACS Appl. Mater. Interfaces*, 2019, **12**: 2417
- [29]. Wang T., Yan F., *Chem. Asian J.*, 2020, **15**: 1524
- [30]. Ferrara C., Patrini M., Pisanu A., Quadrelli P., Milanese C., Tealdi C. and Malavasi L., *J. Mater. Chem. A*, 2017, **5**:9391
- [31]. Luo X., Gao Y., Zhu P., Han Q., Lin R., Gao H., Wang Y., Zhu J., Li S., Tan H., *Solar RRL*, 2020, **4**: 2000169
- [32]. Ryu S., Noh J.H., Jeon N.J., Kim Y.C., Yang W.S., Seo J., Seok S.I., 2014. *Energy Environ. Sci.*, **7**: 2614
- [33]. Gharibzadeh S., Abdollahi Nejad B., Jakoby M., Abzieher T., Hauschild D., Moghadamzadeh S., Schwenzer J.A., Brenner P., Schmager R., Haghghirad A.A., Weinhardt L., *Adv. Energy Mater.*, 2019, **9**:1803699
- [34]. Li J., Hu P., Chen Y., Li Y., Wei M., *ACS Sustain. Chem. Eng.*, 2020, **8**:8624
- [35]. Han Y., Li Y., Wang Y., Cao G., Yue S., Zhang L., Cui B.B., Chen Q., *Adv. Opt. Mater.*, 2020, **8**:1902051
- [36]. Jodlowski A.D., Roldán-Carmona C., Grancini G., Salado M., Ralaizarisoa M., Ahmad S., Koch N., Camacho L., De Miguel G., Nazeeruddin M.K., *Nat. Energy.*, 2017, **2**:972

- [37]. Kaltzoglou A., Antoniadou M., Kontos A.G., Stoumpos C.C., Perganti D., Siranidi E., Raptis V., Trohidou K., Psycharis V., Kanatzidis M.G., Falaras P., *J. Phys. Chem. C*, 2016, **120**:11777
- [38]. Katagiri H., *Thin Solid Films*, 2005, **480**: 426
- [39]. Tsintzos S.I., Pelekanos N.T., Konstantinidis G., Hatzopoulos Z., Savvidis P.G., *Nature*, 2008, **453**:372
- [40]. Chilla J.L., Butterworth S.D., Zeitschel A., Charles J.P., Caprara A.L., Reed M.K., Spinelli L., *Solid State Lasers XIII: Technology and Devices*, 2004, **5332**
- [41]. Zhang Q., Su R., Du W., Liu X., Zhao L., Ha S.T., Xiong Q., *Small Methods*, 2017, **1**:1700163
- [42]. Zhou J., Huang J., *Adv. Sci.*, 2018, **5**:1700256
- [43]. Chakma U., Kumer A., Chakma K.B., Islam M., Howlader D., Mohamed R.M., *Eurasian Chem. Commun.*, 2020, **2**:573
- [44]. Chakma U., Kumer A., Chakma K.B., Islam M., Howlader D., *Adv. J. Chem. A*, 2020, **3**:542
- [45]. Hasan M.M., Kumer A., Chakma U., Islam M.T., *Mol. Simul.*, 2021, **47**:1
- [46]. Islam M.J., Kumer A., *SN Appl. Sci.*, 2020, **2**:251
- [47]. Hasan M.M., Kumer A., Chakma U., *Adv. J. Chem. A*, 2020, **3**:639
- [48]. Islam M.T., Kumer A., Howlader D., Chakma K.B., Chakma U., *Turkish Comput Theor Chem.*, 2020, **4**:24
- [49]. Chakma K.B., Kumer A., Chakma U., Howlader D., Islam M., *Int. J. New Chem.*, 2020, **7**:247
- [50]. Sikder M.M., Chakma U., Kumer A., Islam M.J., Habib A., Alam M.M., *Appl. J. Environ. Eng. Sci.*, 2021, **7**:103
- [51]. Islam M.T., Kumer A., Chakma U., Howlader D., *Orbital: Electron. J. Chem.*, 2021, **13**:58
- [52]. Halali V.V., Rani R.S., Balakrishna R.G., Budagumpi S., *Microchem. J.*, 2020, **156**:104808
- [53]. Li C., Lu J., Zhao Y., Sun L., Wang G., Ma Y., Zhang S., Zhou J., Shen L., Huang W., *Small*, 2019, **15**:1903599
- [54]. Perdew J.P., Burke K., Ernzerhof M., *Phys. Rev. Lett.*, 1996, **77**:3865
- [55]. del Campo J.M., Gázquez J.L., Trickey S.B., Vela A., *J. Chem. Phys.*, 2012, **136**:104108
- [56]. Yang K., Zheng J., Zhao Y., Truhlar D.G., *J. Chem. Phys.*, 2010, **132**:164117
- [57]. Lang L., Yang J.H., Liu H.R., Xiang H.J., Gong X.G., *Phys. Lett. A*, 2014, **378**:290
- [58]. Koopmans T., *Physica*, 1934, **1**:104
- [59]. Kumer A., Sarker N., Paul S., Zannat A., *Adv. J. Chem. A*, 2019, **2**:190
- [60]. Kumer A., Sarker, N., Paul S., *Int. J. Chem. Technol.*, 2019, **3**:26
- [61]. Kumer A., Sarker, N., Paul S., *Turkish Comput. Theor. Chem.*, 2019, **3**:59
- [62]. Kumer A., Sarker M.N., Sunanda, P., 2019. *Eurasian J. Environ. Res.*, **3**:1
- [63]. Shinde R.A., Adole V.A., *J. Appl. Organomet. Chem.*, 2021, **1**: 41
- [64]. Hoque M.M., Kumer A., Hussen M.S., Khan M.W., *Int. J. Adv. Biol. Biomed. Res.*, 2021, **9**:77
- [65]. Kleinman D., *Phys. Rev.*, 1962, **126**:1977
- [66]. Lovell R., *J. Phys. C Solid. State Phys.*, 1974, **7**:4378
- [67]. Smith J.M., *J. Chem. Edu.*, 1950, 584
- [68]. Kedem O., Katchalsky A., *Biochim. Biophys. Acta*, 1958, **27**:229
- [69]. Kaufman L., Cohen M., *Prog. Metal Phys.*, 1958, **7**:165
- [70]. Yang L., Wang Z., Zhou X., Wu X., Han N., Chen Y., *RSC Adv.*, 2018, **8**:41575
- [71]. Taber K.S., *Innov. Sci. Educ. Technol.*, 2013, **8**:391
- [72]. Cheng Y.Q., Ding J., Ma E., *Mater. Res. Lett.*, 2013, **1**:3
- [73]. de Ligny D., Richet P., *Phys. Rev. B*, 1996, **53**:3013

HOW TO CITE THIS ARTICLE

Tomal Hossain, Md. Sayed Hossain, Md. Hazrat Ali, Unesco Chakma, Ajoy Kumer, Mohammad Jahidul Islam. Investigation of Optoelectronics, Thermoelectric, Structural and Photovoltaic Properties of CH₃NH₃SnBr₃ Lead-Free Organic Perovskites, *Chem. Methodol.*, 2021, 5(3) 259-270

DOI: 10.22034/chemm.2021.130180

URL: http://www.chemmethod.com/article_130180.html